


Extracellular nicotinamide phosphoribosyltransferase (eNAMPT) neutralization counteracts T cell immune evasion in breast cancer

Cristina Travelli,¹ Giorgia Colombo ,² Martina Aliotta,¹ Francesca Fagiani,¹ Natalia Fava,¹ Rita De Sanctis,³ Ambra A Grolla,² Joe G N Garcia,⁴ Nausicaa Clemente,⁵ Paola Portararo,⁶ Massimo Costanza,⁷ Fabrizio Condorelli,² Mario Paolo Colombo,⁶ Sabina Sangaletti,⁶ Armando A Genazzani²

To cite: Travelli C, Colombo G, Aliotta M, *et al*. Extracellular nicotinamide phosphoribosyltransferase (eNAMPT) neutralization counteracts T cell immune evasion in breast cancer. *Journal for ImmunoTherapy of Cancer* 2023;**11**:e007010. doi:10.1136/jitc-2023-007010

► Additional supplemental material is published online only. To view, please visit the journal online (<http://dx.doi.org/10.1136/jitc-2023-007010>).

CT and GC contributed equally. SS and AAG contributed equally.

Accepted 04 October 2023



© Author(s) (or their employer(s)) 2023. Re-use permitted under CC BY-NC. No commercial re-use. See rights and permissions. Published by BMJ.

For numbered affiliations see end of article.

Correspondence to

Professor Armando A Genazzani; armando.genazzani@uniupo.it

ABSTRACT

Background Nicotinamide phosphoribosyltransferase (NAMPT) is a key intracellular enzyme that participates in nicotinamide adenine dinucleotide (NAD) homeostasis as well as a released cytokine (eNAMPT) that is elevated in inflammatory conditions and in cancer. In patients with breast cancer, circulating eNAMPT is elevated and its plasma levels correlate with prognosis and staging. In light of this, we investigated the contribution of eNAMPT in triple negative mammary carcinoma progression by investigating the effect of its neutralization via a specific neutralizing monoclonal antibody (C269).

Methods We used female BALB/c mice injected with 4T1 clone 5 cells and female C57BL6 injected with E0771 cells, evaluating tumoral size, spleen weight and number of metastases. We injected two times a week the anti-eNAMPT neutralizing antibody and we sacrificed the mice after 28 days. Harvested tumors were analyzed by histopathology, flow cytometry, western blot, immunohistochemistry, immunofluorescence and RNA sequencing to define tumor characteristics (isolating tumor infiltrating lymphocytes and tumoral cells) and to investigate the molecular mechanisms behind the observed phenotype. Moreover, we dissected the functional relationship between T cells and tumoral cells using three-dimensional (3D) co-cultures.

Results The neutralization of eNAMPT with C269 led to decreased tumor size and reduced number of lung metastases. RNA sequencing and functional assays showed that eNAMPT controlled T-cell response via the programmed death-ligand 1/programmed cell death protein 1 (PD-L1/PD-1) axis and its neutralization led to a restoration of antitumoral immune responses. In particular, eNAMPT neutralization was able to activate CD8⁺IFN γ ⁺GrzB⁺ T cells, reducing the immunosuppressive phenotype of T regulatory cells.

Conclusions These studies indicate for the first time eNAMPT as a novel immunotherapeutic target for triple negative breast cancer.

INTRODUCTION

Immunotherapy has taken the oncological field by storm in the last decade, and cytotoxic

WHAT IS ALREADY KNOWN ON THIS TOPIC

⇒ It is known that extracellular nicotinamide phosphoribosyltransferase (eNAMPT) is elevated in patients with cancer. In breast cancer, high eNAMPT levels after surgery are associated with shorter disease-free survival and overall survival and correlate with TNM (tumor-node-metastasis) staging, tumor size, lymph node metastasis and histological grading, identifying this cytokine as a negative prognostic factor.

WHAT THIS STUDY ADDS

⇒ We generated a neutralizing anti-eNAMPT antibody able to reduce tumor growth, splenomegaly and lung metastases in two different models of triple negative breast cancer. Moreover, the neutralization of eNAMPT reverted the immunosuppressive phenotype of T regulatory cells and activated T cytotoxic cells, thereby counteracting tumoral growth.

HOW THIS STUDY MIGHT AFFECT RESEARCH, PRACTICE OR POLICY

⇒ eNAMPT is involved in tumor growth and its neutralization may represent an efficient target for immunotherapy in triple negative breast cancer.

T-lymphocyte antigen 4 (CTLA-4)-based and programmed death-ligand 1/programmed cell death protein 1 (PD-L1/PD-1)-based therapies have modified prognosis in a number of different cancer settings, from adjuvant to advanced, from melanoma to lymphomas.¹ Alongside, other strategies such as bispecific antibodies, that bring in close proximity the tumor and the immune system,^{2,3} and chimeric antigen receptor (CAR) Ts⁴ have also re-shaped the treatment *scenario*. Both PD-1/PD-L1 and CTLA4-based therapies are based on similar mechanisms: disrupting cell–cell interactions that lead to immune escape.¹ Yet, an alternative immunotherapeutic strategy

would be to disrupt those mechanisms responsible for the expression of the proteins located on the plasma membrane that mediate these cell–cell interactions.¹

Nicotinamide phosphoribosyltransferase (NAMPT) is an intracellular enzyme involved in nicotinamide adenine dinucleotide (NAD) production and it has been previously shown that its inhibition leads to a reduction in tumor growth due to energetic depletion of the cancer cell as well as an effect of myeloid derived suppressor cells.⁵ Yet, this protein can also be secreted, and extracellularly (eNAMPT) acts as a *bona fide* cytokine.^{6–9} eNAMPT is identical to pre-B cell enhancing factor, first described for its ability to synergize with interleukin 7 and stem cell factor, increasing the number of pre-B cell colonies¹⁰ and to visfatin, a cytokine released from adipose tissue.¹¹ Importantly, eNAMPT is elevated in the plasma of patients with cancer and correlates with prognosis.^{12,13} While the specific role of eNAMPT in cancer is still unclear, it is known that it impacts on inflammation, affecting both innate and adaptive immunity.^{14–17} How eNAMPT exerts its extracellular functions has not been fully elucidated.^{16,18,19} Van den Bergh *et al.*¹⁹ proposed a direct binding to C-C chemokine receptor type 5 (CCR5), and we have confirmed that eNAMPT may have an antagonistic role on this receptor.²⁰ Even though data that shows toll-like receptor 4 (TLR4) activation as the primary mechanism of action at present appears more robust,^{18,21} we have recently highlighted that TLR4 is not the sole receptor.¹⁶

The aim of this work was to define the role of eNAMPT in triple negative breast cancer (TNBC), which still has the worst prognosis among breast cancers.²² High eNAMPT levels after surgery are associated with shorter disease-free survival and overall survival²³ and correlate with TNM (tumor-node-metastasis) staging, tumor size, lymph node metastasis and histological grading.²⁴ To dissect the role of this cytokine, we made use of a neutralizing antibody that selectively affects the extracellular protein without affecting cell metabolism.^{13,15} We now show that eNAMPT coordinates the PD-1/PD-L1 axis in tumoral and T cells and that its neutralization leads to the abolishment of PD-1/PD-L1-mediated immune evasion. These studies are highly consistent with eNAMPT as a novel therapeutic target for TNBC.

MATERIALS AND METHODS

Syngeneic orthotopic mammary carcinoma mouse model

Animal care was in compliance with Italian regulations and experiments were authorized by the Ministry of Health (120/2018 DB064.30 of 27/03/2018) and conducted under ARRIVE1 (Animal Research: Reporting of In Vivo Experiments) reporting guidelines.²⁵ Female mice, 8–10 weeks old, were used for all the experimental procedures. BALB/C mice, BALB/c Nude Mouse (Charles Rivers Laboratories) and C57BL/6 (Envigo Laboratories) were maintained under a 12 hours light/dark cycle at 21±1°C and 50±5% humidity. Standard

laboratory diet and tap water were available ad libitum. The 4T1 clone 5 cells²⁶ were maintained in minimum essential medium (MEM) with 10% fetal bovine serum (FBS), 2 mmol/L l-glutamine, and 10 µg/mL penicillin–streptomycin. The EO771 cells (ATCC, CRL-3461) were maintained in Dulbecco's modified eagle medium (DMEM) with 10% FBS, 2 mmol/L l-glutamine, and 10 µg/mL penicillin–streptomycin. A total of 7×10³ 4T1 (or 4T1-GFP) or 5×10⁵ EO771 cells were injected in the fat pad of female BALB/C and C57BL/6 mice, respectively, using a 26-gage needle. Mice were treated intraperitoneally (i.p.) with either vehicle (phosphate-buffered saline (PBS), two times a week), control IgG1 (Mouse IgG1 HKSP84, Ichorbio; 2.5 mg/kg in PBS, two times a week), or C269 (2.5 mg/kg in PBS, two times a week). When not explicitly stated, C269 treatment was performed from day 1 of engraftment (eg, immunoprofiling, RNA sequencing (RNAseq)), in some experiments C269 was given from day 15 after the randomization of mice according to the tumoral mass size in the therapeutic setting. The humanized eNAMPT-neutralizing monoclonal antibody (mAb), ALT-200 (provided by Aqualung Therapeutics), was administered i.p. at a dose of 0.4 mg/kg every 7 days. The αPD-1 (InVivoMab, Bio X Cell, clone RMP1-14) and αPD-L1 (InVivoPlus, Bio X Cell, clone 10F.9G2) were administered i.p. at a dose of 2 mg/kg at days 4, 8 and 12.

Starting from day 15, tumor growth was monitored using a caliper. On day 28, mice were sacrificed, blood was collected, mice were sacrificed, and spleen, primary tumors, and lungs collected. Tumor and spleen weights were measured, lungs were washed in PBS, and lung metastases counted.

Metastasis evaluation

Clonogenic assay

Lungs were removed, minced, and digested with a collagenase IV (Merck Life Science) solution for 140 min 4°C. The suspension was filtered with a cell strainer (Greiner) and centrifuged. Cells were washed and resuspended in DMEM containing thioguanine (10 µg/mL, Merck Life Science) and seeded in 100 mm³ Petri dishes at three dilutions (1:2, 1:10, and 1:100). Colonies were allowed to grow for 2 weeks and then fixed with methanol and stained with crystal violet.

India ink assay

Pulmonary metastases were enumerated by intratracheal injection of India ink (15% India Ink, 85% water, 3 drops NH₄OH/100 mL). India ink injected lungs were washed in Fekete's solution (300 mL 70% EtOH, 30 mL 37% formaldehyde, 5 mL glacial acetic acid). White tumor nodules against a blue lung background were counted.

Stable 4T1-GFP generation

green fluorescent protein (GFP) was cloned in the pLV-IRES-GFP bicistronic vector. The lentiviral particles were produced as described elsewhere²⁷ in HEK293T cells transfected with pMDLg/pRRE, pMD2.VSVG, pRSV-Rev

and pLV-IRES-GFP. Briefly, after 48 hours, cell medium was collected, filtrated and centrifuged for 1 hour 30 min at 100,000×g. The viral particles, corresponding to the pellet fraction, were resuspended and used to infect 4T1 cells, after virus titration. A stable 4T1-GFP cell line was created, GFP expression was monitored with immunocytochemistry and western blot.

Cell isolation for RNA sequencing

After sacrifice, 4T1 clone 5-GFP cells, CD4⁺ and CD8⁺ infiltrating T lymphocytes were isolated from tumoral masses of IgG1-treated and C269-treated mice. First, primary tumors were minced with scissors and disaggregated with collagenase (0.5 mg/mL) for 1 hour in agitation. Single cell suspensions were abrogated of dead cells using Dead Cell Removal Kit (Miltenyi) and CD4⁺ and CD8⁺ infiltrating lymphocytes were positively selected using CD4 and CD8 (tumor infiltrating lymphocytes, TILs) MicroBeads, mouse (Miltenyi). 4T1-GFP cells were positively cell sorted from the single cell suspension (S3e Cell Sorter, Bio-Rad).

After the isolation, cell pellets were washed and RNA was extracted using SPLIT RNA Extraction Kit (Lexogen, Vienna, Austria).

RNA sequencing and data analysis

Libraries were generated from total RNA (five samples/conditions) of 4T1-GFP, CD4⁺ and CD8⁺ infiltrating lymphocytes isolated from tumor form IgG1-treated and C269-treated mice. Total RNA quality was evaluated using the Agilent 2100 Bioanalyzer System.

RNA samples were processed using the QuantSeq 3' mRNA-Seq Library Prep Kit (Lexogen, Vienna, Austria) and sequenced on an Illumina NextSeq 500. Read counts were normalized for effective library size, and differentially expressed genes (DEGs) were analyzed using DESeq V.2.21, DEGs were identified by an false discovery rate (FDR) <0.05 and an absolute fold change >1.

The functional analysis of the identified DEGs was performed with DAVID V.6.8 and Panther Classification System V.12.0 by uploading all the DEGs. The RNAseq data have been deposited in the Gene Expression Omnibus database under the accession GSE223539.

Next, messenger RNA (mRNA) accession numbers of DEGs were subjected to TF binding motif enrichment analysis using enriched groups of -950 base pair sequence to +50 base pair using Pscan²⁸ and the JASPAR database.

Wound healing assay

When confluent monolayers 4T1-clone 5 cells were established, we performed a cross-shaped scratch with tip. Then, the cells were washed twice with PBS to remove residual cell debris. Cells were then incubated with eNAMPT (500 ng/mL), control IgG1 (10 µg/mL), C269 (10 µg/mL) or ALT-200 (10 µg/mL) for 24 hours and photographs of a defined wound spot were taken at different time points. The area of the wound was measured and analyzed using

Image J software (National Institutes of Health, Maryland, USA).

Cell viability assay

To analyze cell viability of 4T1 cells after eNAMPT, control IgG1, C269 and ALT-200 treatments (10 µg/mL), the colorimetric 3-(4,5-dimethylthiazol-2-yl)-2,5-diphenyltetrazolium bromide (MTT) assay was used. Briefly, cells were plated in 24-well plates and treated as indicated for the appropriate time. Vehicle control was added to the cells to give a final concentration no greater than 0.1%. MTT (250 µg/mL in Locke buffer) was added, and cells were incubated for 1 hour at 37°C. Then formazan crystals were dissolved in isopropyl alcohol plus 0.1 m HCl. The absorbance was read at 570 nm in a plate reader (Victor3 V, PerkinElmer Life Sciences).

T-cell isolation

T cells were isolated from the spleen of healthy mice using naive CD4⁺ and CD8⁺ T Cell Isolation Kit mouse (Miltenyi) and used for *in vitro* experiments. Regulatory T cells (Tregs) for suppression assays were obtained sorting CD4⁺CD25⁺ cells from tumor lysates (online supplemental figure 6 for the gating strategy).

3D culture and co-culture

4T1 spheroids were generated by seeding 10⁴ cells per well on V-96 wells plates in complete MEM and 5 days later, spheroids were co-cultured with 3×10⁵ CD4⁺, CD8⁺ or CD4⁺/CD8⁺ cells per well, together with control IgG1 or C269 and 6 wells per condition were seeded. For quantitative PCR (qPCR) and flow cytometry analysis OUT and IN compartments were isolated by first pooling the 6 co-cultured wells in 1.5 mL tubes. Spheroids were gently resuspended and left to sediment to the bottom of the 1.5 mL tubes. Supernatant cell suspension constitutes the non-infiltrating immune cells (=OUT). These steps were repeated two times with PBS to wash the spheroids from the non-infiltrating immune cells. Spheroids were then trypsinized to obtain a single cell suspension (=IN) further analyzed by qPCR flow cytometry.

Spheroid volume calculation

Before trypsinization, pooled spheroids were placed in 96-well plates and pictured using the Leica THUNDER Imager 3D Live Cell microscope, Wetzlar, Germany (Objective 5×). Images were then analyzed using the Icy software by measuring the length (L) and width (W) of each spheroid. Spheroid volumes were then calculated as follows: $V = (L \times W \times W) / 2$ as reported in a study by Courau *et al.*²⁹

T-cell infiltration calculation

4T1-GFP cells and isolated T cells labeled with Cell-Tracker Red CMTPX Dye (Thermo Fisher Scientific) were co-cultured for the evaluation of T lymphocyte infiltration as previously described. Images were taken with Leica THUNDER Imager 3D Live Cell microscope,

Wetzlar, German (Objective 5×) and region of interests (ROIs) were calculated using Icy software.

T-cell proliferation and suppression assays

Lymph nodes and spleen cells from IgG1-treated and C269-treated mice were harvested and processed to obtain a single cell suspension. CD3⁺ T cells were purified from suspensions depleted of B220, CD11b, CD49b, and Ter-119-positive cells by sorting CD4⁺CD25⁺ cells from tumor lysates (online supplemental figure 6, for the gating strategy). CD3⁺ T cells (50×10³/well) were stimulated in a 96-well plate with anti-CD3 antibody (1 µg/mL), or medium alone in enriched Roswell Park Memorial Institute (RPMI) 1640 medium in the presence of 500×10³ splenocytes from naïve mice as an antigen presenting cell (APC) source. After 72 hours of incubation (37°C, 5% CO₂), cultures were pulsed for 18 hours with 0.5 µCi/well [H3]-thymidine, and proliferation was measured from triplicate cultures on a β-counter (Perkin Elmer, Waltham, Massachusetts, USA). Data are shown as mean cpm±sem.

Flow cytometry

Primary tumors were minced with scissors and disaggregated with collagenase (0.5 mg/mL) for 1 hour in agitation. Cells (10⁶) were resuspended in Hank's Balanced Salt Solution with 0.5% bovine serum albumin (BSA) and staining was performed at 4°C for 30 min with specific antibodies (see online supplemental table 1). Cell viability was determined by LIVE/DEAD Fixable Violet Dead Cell Stain Kit. For intracellular staining, Foxp3/Transcription Factor Staining Buffer Set was used according to the manufacturer's instructions. Cells were detected using the BD FACSCanto II or BD FACSymphony A5 and analyzed with BD FACSDiva and FlowJo (9.3.2) software.

For spheroids evaluated throughflow cytometry, cells were stained in 0.5% FBS and 1 mM EDTA in Hank's balanced salt solutions (HBSS) solution with the antibodies reported in online supplemental table 2. Cell viability was determined by BD Horizon Fixable viability stain. For intracellular staining, BD Cytfix/Cytoperm Fixation/Permeabilization Solution Kit was used according to the manufacturer's instructions. Cells were acquired using BD Symphony, and data were analyzed using BD FACSDiva V.8.0.2 and FlowJo (10.6.1) software.

Gene Expression Analysis

Cells were lysed with Trizol reagent (Life Technologies) and RNA was extracted with chloroform. 1 µg RNA was reverse transcribed with SENSIFAST kit as manufacturer's protocol (Aurogene) and 20 ng of cDNA were used to perform qPCR with SYBR-green (Bio-Rad) and CFX96 Real-Time System (Bio-Rad). Gene expression results were normalized to actin as housekeeping gene. The sequences of gene-specific primers are reported in online supplemental table 2.

Immunohistochemical and immunofluorescence analysis

At the end of the experiment mice were euthanized and the tumors were resected. 4 µm-thick tissue sections of tumors were deparaffinized, rehydrated and unmasked using Novocastra Epitope Retrieval Solutions in a thermostatic bath at 95°C for 15 min. Next, the sections were brought to room temperature and washed in PBS. After neutralization of the endogenous peroxidase with H₂O₂ and Fc blocking by a specific protein solution, samples were incubated overnight with primary antibodies at 4°C. Staining was revealed using IgG (H&L) specific secondary antibodies (Life Technologies) and 3–3' diaminobenzidine (DAB) chromogenic substrate. The slides were counterstained with Harris haematoxylin (Novocastra). Sections were analyzed using a Leica DM4 B optical microscope equipped with a Leica DFC450 digital camera.

Immunofluorescence analyses were performed on frozen optimal cutting temperature (OCT) compound-embedded samples. For granzyme b intracellular staining, 4 µm-thick sections were fixed with 4% paraformaldehyde and permeabilized with 0.1% triton x-100. For cell membrane staining, sections were fixed with cold acetone. Sections were blocked in pbs 1x with 5% bsa and incubated with primary antibody for 1 hour. Nuclei were counterstained with the 4',6-diamidino-2-phenylindole (dapi) stain. All confocal microscopy analyses were performed using a leica tcs-sp8-x confocal laser scanning microscope.

eNAMPT-neutralizing murine (C269) and humanized mAbs (ALT-200)

The generation and purification of the murine anti-eNAMPT antibody (C269) was previously described in.¹⁵ The humanized eNAMPT-neutralizing mAb ALT-200 mAb, was provided by Aqualung Therapeutics Corporation, Tucson, Arizona, USA.^{13 30 31}

Western blot analysis

4T1 cells and primary tumors were lysed in Lysis Buffer (20 mM HEPES, 100 mM NaCl, 5 mM EDTA, 1% Nonidet-P40⁺ Protease & Phosphatase Inhibitor Cocktail, Sigma). Proteins quantification was performed with Bradford Protein Assay (Sigma), and proteins were resolved on SDS-PAGE and transferred with TurboBlot system (Bio-Rad, Hemel Hempstead, UK). Proteins were detected with primary antibodies and peroxidase-conjugated secondary antibodies (Bio-Rad) and resolved by chemiluminescence analysis using ECL (Thermo Fisher Scientific). Densitometry analysis was performed with the Image Lab program (Bio-Rad, Hemel Hempstead, UK). The mouse anti-βactin A1978 antibody was from Sigma, the rabbit CTLA4 clone VU-ID9 antibody and the rabbit ICOS antibody were from biorbyt, the rabbit ICOSL antibody was from abbexa, the rabbit anti-PD-1/CD279 Polyclonal antibody 66 220–1-Ig and anti-PD-L1/CD274 monoclonal antibody 66 248–1-Ig were from Proteintech.

Recombinant NAMPT production

Recombinant endotoxin free-NAMPT was generated and purified in house as previously described.^{15,32}

ELISA

Serum eNAMPT was evaluated with a commercially available sandwich ELISA for murine NAMPT (ELISA kit from AdipoGen; Seoul Korea).

Statistics

Data are presented as mean±SEM. The normality of data distributions was evaluated using the Shapiro-Wilk test. Parametric (unpaired t-test and one-way analysis of variance followed by Tukey's post-hoc) or non-parametric (Mann-Whitney U test and one-way Kruskal-Wallis H test followed by Dunn's post-hoc statistical analysis) was used. All statistical assessments were two-sided and a value of $p < 0.05$ was considered statistically significant. Statistical analysis was performed using GraphPad Prism software (GraphPad Software, USA).

RESULTS

Neutralisation of eNAMPT reduces TNBC growth *in vivo*

To investigate the contribution of eNAMPT in the progression of TNBC, we first investigated the effect of the murine eNAMPT-neutralizing antibody C269 (IgG1k,^{15,16}) in 4T1 mouse allografts. Mice were treated with C269 twice a week (2.5 mg/kg, i.p.) starting from day 1 post-implantation (figure 1A). In analogy to patients with breast cancer,¹² serum levels of eNAMPT in implanted mice increased over 10-fold (figure 1B) at day 28 compared with healthy mice. In contrast, mice receiving C269 exhibited markedly reduced serum eNAMPT. Tumors treated with C269 showed a significant reduction of both volume (median 0.45 cm³ vs 0.17 cm³) and weight (median 640.6 mg vs 435.7 mg, figure 1C–E). Alongside, the splenomegaly observed in the implanted mice was also significantly reduced by treatment (figure 1F). Moreover, C269 treatment was able to significantly reduce the number of lung metastases, as assessed by the clonogenic assay (figure 1G). Importantly, C269 was effective to the same extent also when administered when the tumor was palpable (approximately 14–16 days after implantation mice were randomized and treated, figure 1H), causing a significant reduction in tumor volume (median 0.36 cm³ vs 0.10 cm³) and weight (median 486.5 mg vs 368 mg, figure 1I,J), splenomegaly (figure 1K), circulating eNAMPT levels (figure 1L) and lung metastases (figure 1M). While from the raw data the effect of C269 would appear as higher when the treatment starts when the tumor is palpable compared with an early treatment, there was no statistical difference between the two treatments and the data supports the claim that C269 is equally effective in the two regimens. Notably, mock treatment with a non-specific IgG1 had no effect on tumor growth compared with vehicle (online supplemental figure 1A–E).

Since the number of lung metastases could be influenced by the size of the original tumor mass, we injected an identical number of 4T1 cells in the tail vein of treated and untreated mice for 28 days in order to cause immediate dissemination of the transplanted tumoral cells. In such conditions, the number of metastases formed in C269-treated mice was significantly lower than that of the control counterpart (figure 1N).

To confirm that TNBC was sensitive to eNAMPT neutralization, we investigated (1) the effect of C269 in a second TNBC allograft (EO771, online supplemental figure 1F); and (2) the effect of a distinct humanized eNAMPT-neutralizing antibody. As expected, also the EO771 model was characterized by high levels of serum eNAMPT (online supplemental figure 1G) with the effect of C269 on EO771 resembling that on 4T1 (online supplemental figure 1H and I), except for splenomegaly, which is not present in this model (online supplemental figure 1J). A further confirmation was provided by the efficacy of ALT-200 mAb, a distinct anti-eNAMPT antibody,^{13,30,31} on 4T1 allografts (online supplemental figure 1K–O).

eNAMPT does not cell-autonomously control tumoral cell growth *in vitro*

To test whether eNAMPT cell-autonomously sustained tumor cell proliferation or protected from cell death, we exposed cultured 4T1 cells to recombinant murine NAMPT (rNAMPT). Administration of rNAMPT did not alter 4T1 proliferation *in vitro* in traditional monolayer plating (online supplemental figure 2A) at any of the tested times (24–96 hours) or concentrations (10 ng/mL to 1 µg/mL). Similarly, no effect was observed in 4T1 spheroids (online supplemental figure 2B). Since 4T1 cells secrete high amounts of eNAMPT (2.8 ng accumulated in 24 hours from 1 million cultured cells as determined by ELISA and confirmed by western blotting), it is possible that this masks the effect of additional eNAMPT. Yet, no effect on proliferation/cell death was observed when monolayers or spheroids were treated with either of the two eNAMPT neutralizing antibodies (C269 or ALT-200; online supplemental figure 2C–E) at any of the tested times (24–96 hours). eNAMPT neutralization modifies the transcriptional signature of 4T1 cells

We next performed RNA-sequencing on 4T1 cells extracted from tumors after 28 days of treatment with either control IgG1 or C269, administered from day 1. To have a pure sample of tumoral cells, in this set of experiments 4T1 cells were engineered to constitutively express GFP (GFP-4T1, figure 2A), which allowed separation by cell sorting. These cells responded to treatment with C269 in an identical manner to wild-type 4T1 cells in terms of tumor growth, weight, splenomegaly and lung metastasis (online supplemental figure 2F–I).

As compared with IgG1-treated tumors, C269 upregulated 1351 genes and downregulated 1383 genes (figure 2B), using a log₂ fold-change threshold of at least one with an FDR below 0.05. The data set was validated qualitatively and quantitatively by real-time PCR

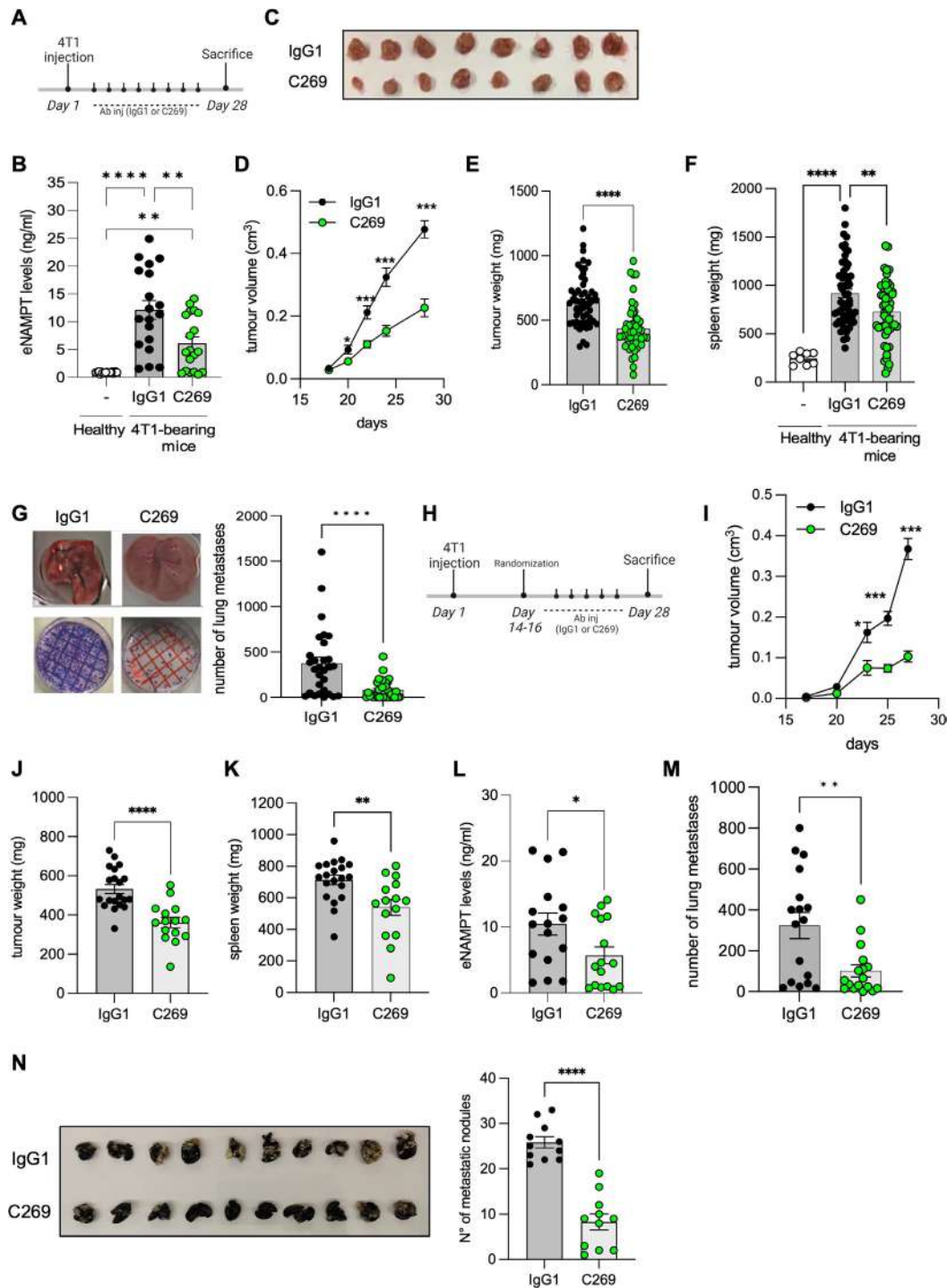


Figure 1 Neutralization of eNAMPT reduces 4T1 tumor growth and metastases. (A) Scheme of the treatment for data presented in panels B–G. 4T1 cells were established intramammary in female BALB/c mice. Control IgG1 (2.5 mg/kg i.p., two times a week) or C269 (2.5 mg/kg i.p., two times a week) were injected intraperitoneally. Data on untreated 4T1-bearing mice is present in online supplemental figure 1. No differences were found compared with IgG1-treated. (B) Serum eNAMPT levels in healthy, IgG1 or C269-treated 4T1-bearing mice. (C) Representative image of 4T1 tumor masses. (D) Tumor volume throughout the course of the experiment. (E) Tumor weight at sacrifice. (F) Spleen weight at sacrifice and in mice of the same age and weight. (G) Lung metastasis determined by the 6-thioguanine clonogenicity assay. Mean±SEM of eight independent experiments. (H) Scheme of the treatment for experiments presented in panels I–M. Control IgG1 (2.5 mg/kg i.p., two times a week) or C269 (2.5 mg/kg i.p., two times a week) were injected intraperitoneally when the tumors were palpable (around day 15). (I) Tumor growth determined by volume throughout the course of the experiment. (J) Tumor weight at sacrifice. (K) Spleen weight at sacrifice. (L) Serum eNAMPT levels at sacrifice. (M) Lung metastasis of 4T1 tumor cells determined by the 6-thioguanine clonogenicity assay. (N) Number of lung metastasis nodules from mice that received tail vein injection of 4T1 in presence or absence of C269. Mean±SEM of three (panels H–N) independent experiments. P value: * $p < 0.05$; ** $p < 0.01$; *** $p < 0.001$, **** $p < 0.0001$. eNAMPT, extracellular nicotinamide phosphoribosyltransferase; i.p., intraperitoneal.

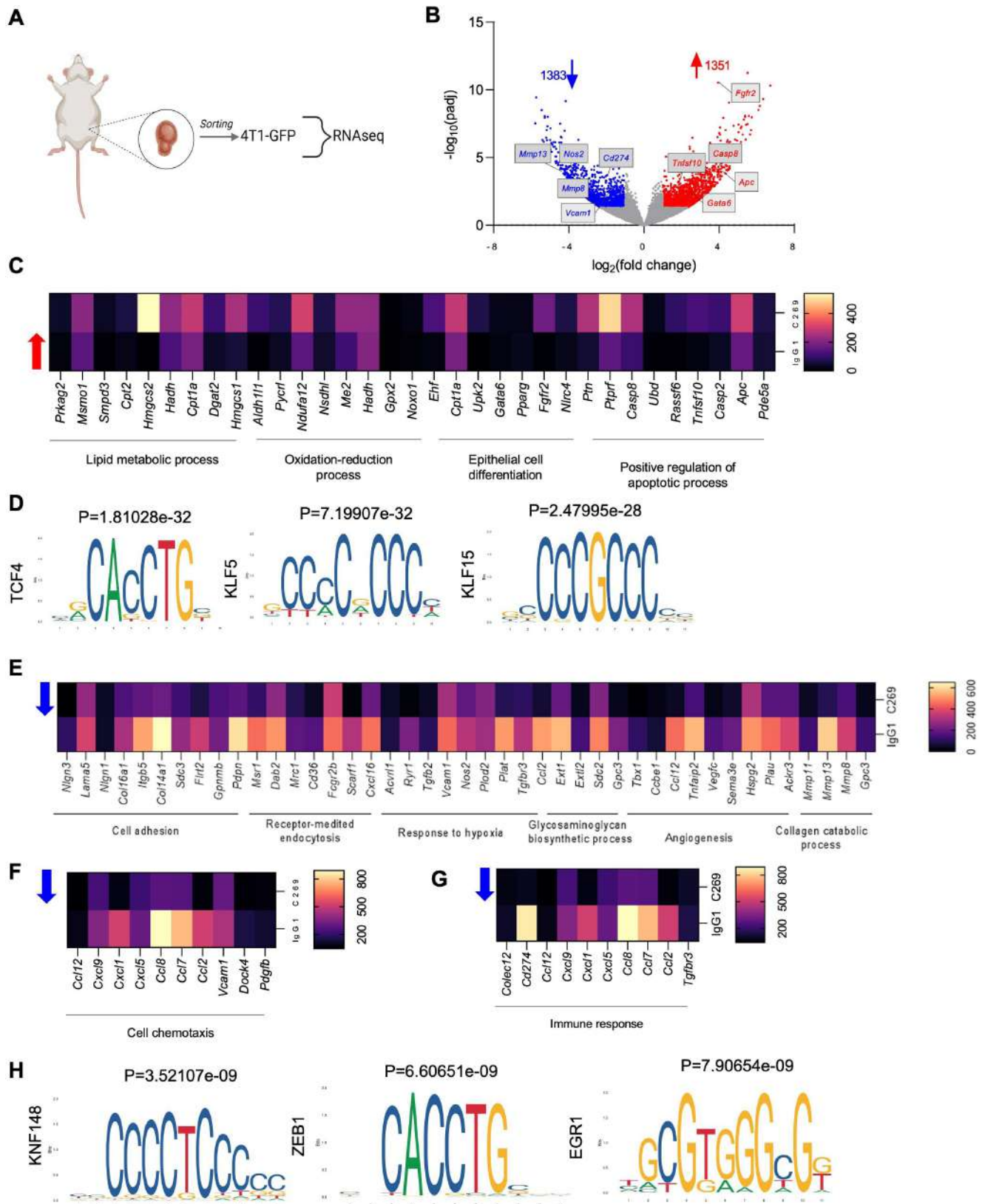


Figure 2 Transcriptomic analysis of 4T1 cells from tumor explants. (A) Representative scheme of cells isolated from 4T1 tumor masses and subjected to RNAseq analysis. (B) Volcano plot of the differentially expressed genes in 4T1clone5-GFP cells ($n=5$ replicates/condition); $\text{FDR} \leq 0.05$. (C) Heat map and histogram depicting the upregulated genes by C269 treatment and relative GO analysis. (D) Patterns of transcription factor motif enrichment within the promoters of the C269-treated 4T1 cell-upregulated genes. (E–G) Heat map and histogram representation depicting the downregulated genes by the C269 treatment and relative GO analysis. (H) Patterns of transcription factor motif enrichment within the promoters of the C269-treated 4T1 cell-downregulated genes. FDR, false discovery rate; GO, gene ontology; RNAseq, RNA sequencing.

on GFP-4T1 clone 5 cells isolated from tumors (online supplemental figure 3A) with a correlation of 0.94. Online supplemental figure 3B lists the most upregulated genes and figure 2C shows the heat map of the top four most enriched upregulated pathways by C269 (ie, when depleting eNAMPT) using gene ontology (GO) analysis. To verify whether this upregulation was cell autonomous or context-dependent, cultured 4T1 cells were treated with rNAMPT and evaluated for changes in the expression of those genes found to be more modulated *in vivo*. Some of these modifications were confirmed also in 4T1 cell cultures (eg, *Gata6*, *Ptn*), while others, and in particular those relating to apoptosis (*Casp2*, *Casp8*, *APC*, online supplemental figure 3C), were not. Transcription factor analysis of DEGs using Pscan and JASPAR suggested that TCF4, KLF5 and KLF15 might be the transcription factors most likely involved (figure 2D).

Online supplemental figure 3D shows the most downregulated genes by C269 (ie, eNAMPT-dependent) and figure 2E–G highlight the top eight most enriched pathways. The most enriched transcription factors in this set of genes were KNF148, ZEB1 and EGR1 (figure 3H). A striking element is represented by the downregulation of genes involved in chemotaxis and cell adhesion, which might correlate with the lower metastatic potential of C269-treated tumors or isolated cells (figure 1G and figure 1N). In this instance most of these changes appeared cell-autonomous, as 11 out of 13 tested genes were directly up-regulated also in 4T1 monolayers on rNAMPT treatment, although 2 (*Lama5* and *Mmp11*) were not (online supplemental figure 3E), suggesting that both mechanisms occur but that eNAMPT has an important direct effect on the cancer cell. To create a functional validation of the transcriptomic data and of this conclusion, we investigated the effect of eNAMPT and C269 on wound closure in cultured 4T1 cells. Treatment *in vitro* with rNAMPT dose-dependently increased the migration of 4T1 cells in the wound (online supplemental figure 3F) while both C269 and ALT-200 mAbs reduced basal 4T1 migration (online supplemental figure 3G,H), suggesting that eNAMPT secreted by mammary carcinoma cells is an autocrine signal for migration.

eNAMPT neutralisation skews T-cell commitment

Analysis of the RNAseq data from GFP-4T1 cells isolated from tumors provided evidence also of an enrichment of genes related to immune-tumor crosstalk (eg, CD274, coding for PD-L1) among those highly downregulated on treatment with C269 (figure 2G). This modulation was cell autonomous as *in vitro* administration of rNAMPT to cultured 4T1 cells also increased PD-L1 transcript (figure 3A) and protein levels (figure 3B,C, online supplemental figure 4A), an effect that was antagonized by co-incubation with C269 (figure 3A–B and E), without any effect on ICOS-L expression (figure 3D,F). This antagonistic effect of C269 on tumoral PD-L1 protein expression was confirmed also *in vivo* on whole tumor homogenates, in 4T1 (figure 3G–J) and EO771

allografts (online supplemental figure 4B). Interestingly, in both 4T1 and EO771 tumor homogenates the decrease in PD-L1 was paralleled by a concomitant decrease in PD-1 (figure 4A,C and online supplemental figure 4B and C), without affecting ICOS expression (figure 4B,D).

As PD-1 is expressed by immune-competent cells (mainly T and pro-B lymphocytes), we next analyzed, throughflow cytometry, both myeloid and lymphoid immune populations extracted from tumors after 28 days, in which control IgG1 and C269 were injected from day 1. While myeloid and B cell compartments did not show any significant modification (online supplemental figure 4C,D) on C269 treatment, substantial differences were observed in the composition of the lymphoid population. In detail, the frequency of CD4⁺ (CD4⁺CD25^{neg}) effector cells were significantly increased in tumors treated with C269 versus control, with no difference in the frequency of T regulatory (CD4⁺CD25⁺FoxP3⁺; figure 4E) or CD8⁺ cells. Thus, we decided to explore more in deep the activation phenotype of T effector cells (Teff), Treg and CD8⁺ cells in response to eNAMPT neutralization. Tumors treated with C269 displayed a decreased frequency of CD4⁺CD25⁺FoxP3⁺PD-1⁺ cells and CD8⁺PD-1⁺ T cells (figure 4F). This was paralleled by a concomitant increase of CD4⁺CD25⁺FoxP3⁺PD-1^{low} Tregs (figure 4G) and of CD8⁺ IFN⁺ GrzB⁺ T cytotoxic cells (figure 4H). No differences were instead found in the CD73⁺ and OX40⁺ subpopulations of Teff (CD4⁺CD62⁺), Treg (CD4⁺CD25⁺FoxP3⁺) and CD8⁺ cells (online supplemental figure 4E,F). To confirm that neutralization of eNAMPT induced a reshaping of T cells, we also performed FACS analysis of EO771 tumors treated with C269. As shown in online supplemental figure 5, the key features of this T-cell reprogramming were confirmed also in this model, that is, an overall increase of CD4⁺ Teffs, a reduction of PD-1⁺ Tregs, an increase of PD-1^{low} Tregs and an increase of CD8⁺ IFN⁺ GrzB⁺ T cytotoxic cells. The above data would suggest that treatment with C269 leads to a more cytotoxic phenotype of CD8⁺ cells. Indeed, this is supported by the observation that, in immunohistochemistry, CD8⁺ cells in the presence of C269 infiltrated deeper in the stroma compared with what is observed in untreated tumors (figure 4I), and that in immunofluorescence it can be ascertained that these cells are granzyme B (GrzB⁺) (figure 4J), thereby confirming their cytotoxic activity. For Tregs, instead, the above data is in principle more controversial, as C269 increased the frequency Treg PD-1^{low}, which has been reported to be more immunosuppressive.³³ In order to ascertain what the overall effect of C269 on Treg was, we isolated CD4⁺CD25⁺ from spleen and from draining lymph nodes of 4T1-bearing mice treated or untreated with C269 and performed a [³H]-thymidine incorporation assay. As shown in figure 3K, total Treg cells derived from C269-treated mice increased [³H]-thymidine incorporation, thereby showing a lower immunosuppressive phenotype (see online supplemental file 6 for gating strategy).

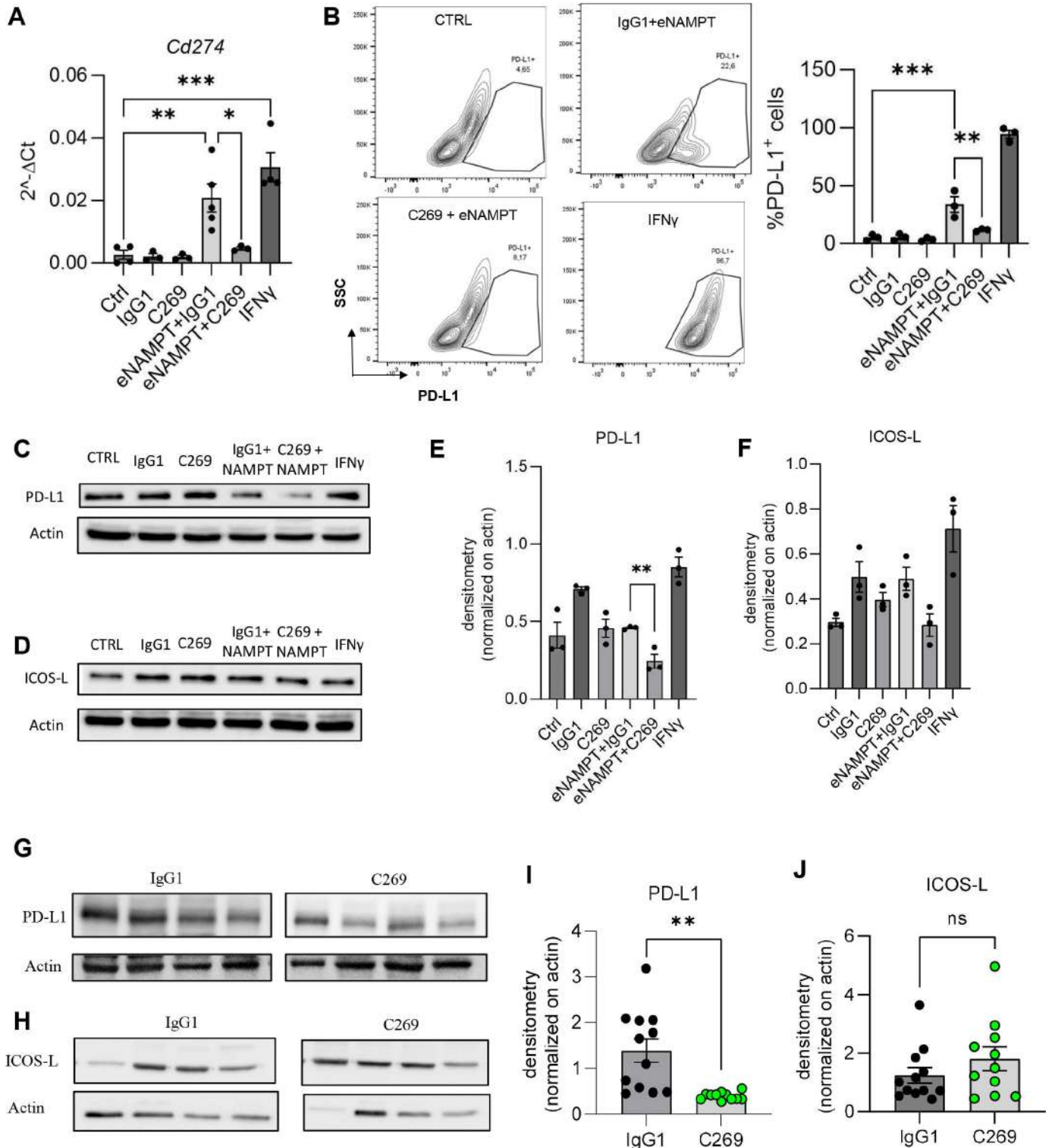


Figure 3 Neutralization of eNAMPT affects the PD-L1 axis in the tumor cells. (A–B) *Cd274* and PD-L1 expression by qPCR and FACS of 4T1 cells in response to eNAMPT (500 ng/mL) or eNAMPT and C269 (10 μ g/mL). IFN γ (100 ng/mL) was used as a positive control. Mean \pm SEM of three independent experiments. (C–D) Representative western blot and (E–F) densitometry of PD-L1 and ICOS-L in total cell lysates of 4T1 treated or not with rNAMPT for 24 hours. Mean \pm SEM of three independent experiments. (G–H) Representative western blot and (I–J) densitometry of PD-L1 and ICOS-L in homogenates from tumors of 4T1-bearing mice. Mean \pm SEM of 12 samples from two independent experiments. eNAMPT, extracellular nicotinamide phosphoribosyltransferase; FACS, fluorescence activated cell sorting; ICOS, inducible T-cell costimulator; IFN, interferon; PD-L1, programmed death-ligand 1; qPCR, quantitative PCR; rNAMPT, recombinant murine NAMPT; SSC, side scatter.

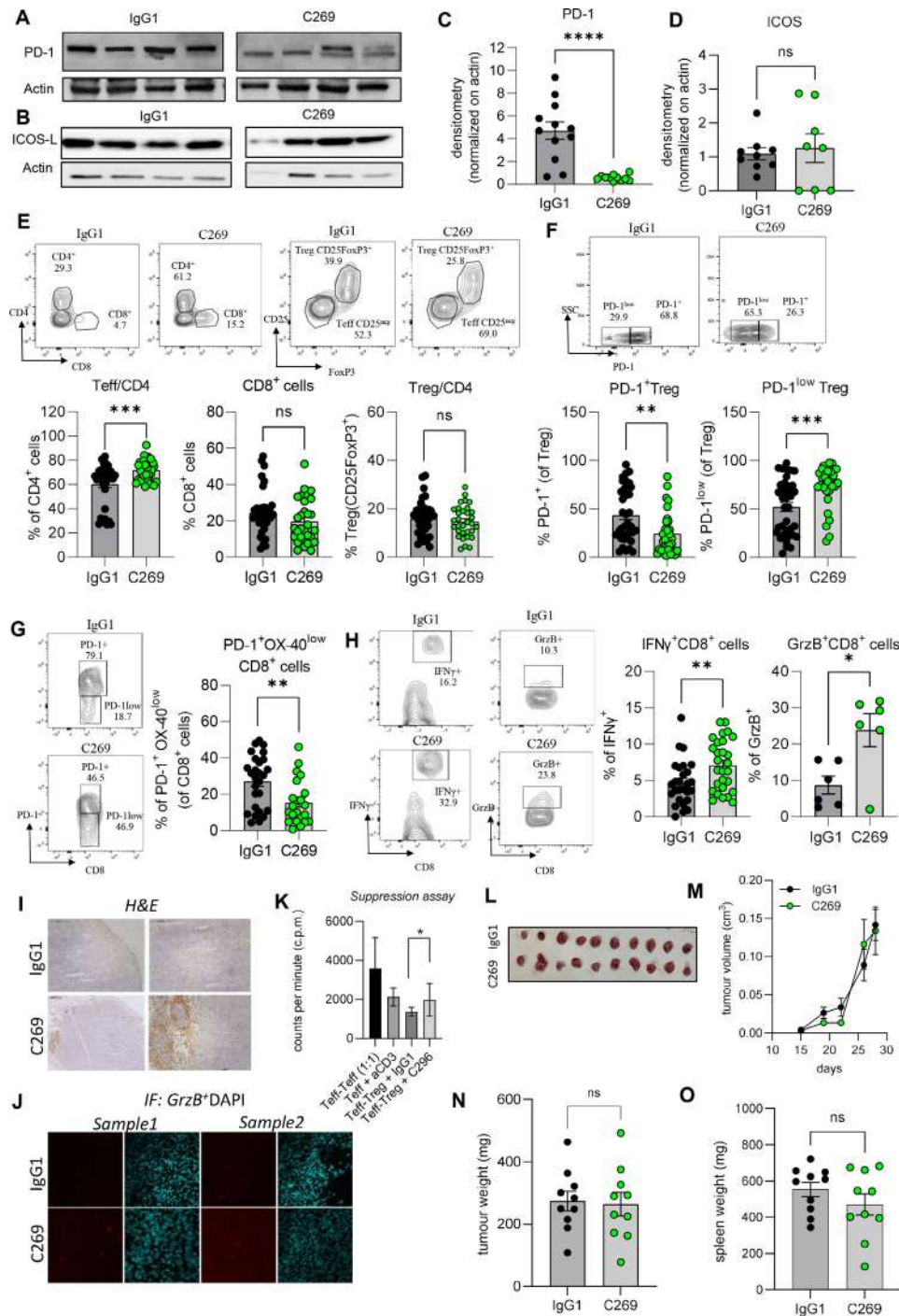


Figure 4 Neutralization of eNAMPT affects the PD-1/PD-L1 axis in the tumor microenvironment. (A–B) Representative western blot and (C–D) densitometry of PD-1 and ICOS in homogenates from tumors of 4T1-bearing mice. Mean \pm SEM of 12 samples from two independent experiments. (E–H) Quantification of: (E) T effector cells, T regulatory cells (gated on CD4⁺ cells) and CD8⁺ cells; (F) PD-1⁺ T regulatory cells (gated on CD4⁺CD25⁺FoxP3⁺); (G) PD-1^{hi}CD8⁺ T cells (gated on CD8⁺ cells); (H) IFN γ ⁺CD8⁺ and GrzB⁺CD8⁺ T cells (gated on CD8⁺ cells) from tumor of 4T1-bearing mice. Mean \pm SEM of five independent experiments. (I) IHC staining of CD8⁺ T cells in 4T1 tumor sections of 4T1-bearing mice. (J) Representative immunofluorescence analysis of GrzB⁺ in CD8⁺ T cells. (K) Suppression assay via [³H]-thymidine incorporation from spleen and draining lymph nodes. Mean \pm SEM of three independent experiments. P value: *p<0.05; **p<0.01; ***p<0.001, ****p<0.0001. (L–O) 4T1 cells were established intramammary in female nude BALB/c mice. Control IgG1 (2.5 mg/kg i.p., two times a week) or C269 (2.5 mg/kg i.p., two times a week) were injected intraperitoneally. (L) Representative image of 4T1 tumor masses. (M) Tumor volume throughout the course of the experiment. (N) Tumor weight at sacrifice. (O) Spleen weight at sacrifice and in mice of the same age and weight. Mean \pm SEM of one experiment. DAPI, 4',6-diamidino-2-phenylindole; eNAMPT, extracellular nicotinamide phosphoribosyltransferase; GrzB, granzyme B; ICOS-L, inducible costimulator-ligand; IFN, interferon; IHC, immunohistochemistry; i.p., intraperitoneal; PD-1, programmed cell death protein 1; PD-L1, programmed death-ligand 1; Teff, T effector cells; Treg, regulatory T cell.

If the above hypotheses linking eNAMPT to T-cells were correct, it could be expected that 4T1 engraftment in Balb/c nude mice would be partially or fully resistant to C269 treatment. Reassuringly, tumors grew to the same extent in the presence or absence of C269 in NGS mice (administered from engraftment), and no changes in tumor weight or in spleen size was observed (figure 4L–O). T-lymphocytes, therefore, are indispensable to disclose an effect of eNAMPT neutralization.

eNAMPT controls T-cell infiltration and activation

To provide an insight into the mechanism responsible for the changes described above, we purified CD4⁺ and CD8⁺ cells from 4T1 tumors and performed RNAseq (figure 5A). By using a log₂ fold-change threshold of at least one with an FDR below 0.05, we observed that C269 treatment upregulated 65 and 112 genes in CD4⁺ and in CD8⁺ cells, respectively, while causing downregulation of 158 and 92 genes. These data were confirmed by real-time PCR on isolated lymphocytes from tumors (online supplemental figure 7A) with a correlation of 0.84.

Online supplemental figure 7B and figure 5B shows the heat map of the top two most enriched downregulated pathways by C269 in isolated CD4⁺ T cells (ie, when depleting eNAMPT) using GO analysis. In accordance with all the data described above, we found an enrichment in the genes associated with the PD-1 pathway. No significant downregulated pathway in CD4⁺ cells emerged. Online supplemental figure 7C and figure 5C highlight the only enriched pathway from upregulated genes in CD8⁺ T cells. Again, in accord to the *in vivo* effect of C269 and to the flow cytometry analysis, the gene signature is linked to cytotoxic T-cell activity. Overall, the above data show that eNAMPT depletion in tumor-bearing mice leads to a selective ablation of the PD-1 axis and the reactivation of cytotoxicity.

These effects may be attributed to a direct action of circulating eNAMPT on immune cells, on the basis of experiments conducted with rNAMPT on lymphocytes isolated from healthy mice. Indeed, in CD4⁺ and CD8⁺ cells, rNAMPT (500 ng/mL for 24 hours) induced a significant increase in PD-1 transcripts which was paralleled by an increase in the expression of the protein (figure 5D–F). These data are corroborated by the observation that treatment of naïve lymphocytes (CD4⁺ and CD8⁺) with eNAMPT for 48 hours leads to an increase in PD-1. When these cells are incubated for 24 hours with eNAMPT and then for a further 24 hours also with C269, this increase is abolished both on CD4⁺ and CD8⁺ cells (figure 5G). Similarly, and in accord to the overall actions of eNAMPT on lymphocytes, rNAMPT induced an upregulation of *Cxcl1*, *Cxcl9*, *Il6* and *Hif1a* on CD4⁺ and an upregulation of *Ifng*, *Il6* and *Cxcl11* on CD8⁺ (online supplemental figure 7D).

If a link exists between eNAMPT and the PD-1/PD-L1 axis, it would be expected that inhibiting both pathways would not yield a synergic or additive effect. To this end, we treated 4T1-bearing mice after 4, 8, and 12 days of

engraftment with an anti-PD-1 (2 mg/kg) or anti-PD-L1 (2 mg/Kg) antibody and with C269 (every 3 days, as for all other experiments). Inhibiting PD-1 alone yielded a modest but statistically significant reduction in tumor volume and in lung metastases (online supplemental figure 8A–C), while inhibiting PD-L1 alone yielded a non-significant volume reduction but a significant reduction in metastases (online supplemental figure 8A–C). The modest effect of anti-PD-1/PD-L1 on the primary tumor was expected, reported also by others and in line with a modest effect yet clinically relevant seen in triple negative patients treated with immunotherapy.³⁴ Supporting our hypotheses, co-treatment did not show any additiveness with either antibody (online supplemental figure 8A–C). On the contrary, and unexpectedly, both anti-PD-1 and PD-L1 reversed the effect of C269 on the primary tumor, although this did not occur for lung metastases. This would imply that inhibiting the PD-1/PD-L1 axis affects the eNAMPT cascade, and indeed both antibodies significantly reduced the levels of the cytokine (online supplemental figure 8D).

To explore whether eNAMPT affected solely the PD-1/PD-L1 axis, we manually searched the RNAseq CD4⁺ and CD8⁺ data sets for changes in other checkpoint genes (*Tim3*, *Lag3*, *Icos*, *Ctla4* or *Ox40*, online supplemental figure 7E) and alongside verified any change by qPCR on lymphocytes from tumors. No significant changes were observed. Alongside, no changes were observed in *Icosl*, *Cd274* and *Cxcr4* on 4T1 from tumors, highlighting a specific regulation of the PD-1/PD-L1 axis (online supplemental figure 7F). This was confirmed by western blot (WB) and FACS analyses (online supplemental figure 7G–H).

To give functional significance to the transcriptional changes documented in tumor-isolated CD4⁺ and CD8⁺ cells, we recreated an *in vitro* model of tumor-induced immunological challenge using mixed (4T1-T lymphocytes) three-dimensional cultures. Thus, CD4⁺, CD8⁺ or CD4⁺/CD8⁺ cells were pretreated for 24 hours with rNAMPT, then washed and incubated with untreated 4T1 spheroids (figure 6A). When rNAMPT-primed T-lymphocytes were incubated with naïve 4T1 spheroids, infiltration of CD4⁺ cells was statistically increased as documented by immunofluorescence (figure 6B,C) and flow cytometry (figure 6D). We further decided to characterize these primed lymphocytes for PD-1 expression and found an increased expression in total CD4⁺ cells and in Treg (CD4⁺CD25⁺FoxP3⁺), while no large difference was observed in the PD-1 expression of CD8⁺ cells, nor of other functional marker (online supplemental figure 9). The increased infiltration, therefore, does not depend on PD-1 expression. The number of 4T1 cells in the spheroids was unchanged.

Next, we decided to investigate how neutralizing eNAMPT with C269 disrupted this setting by incubating lymphocytes with 4T1 spheroids in the presence or absence of C269 and relying on the endogenous eNAMPT released from the spheroid. As shown in figure 6F,G,

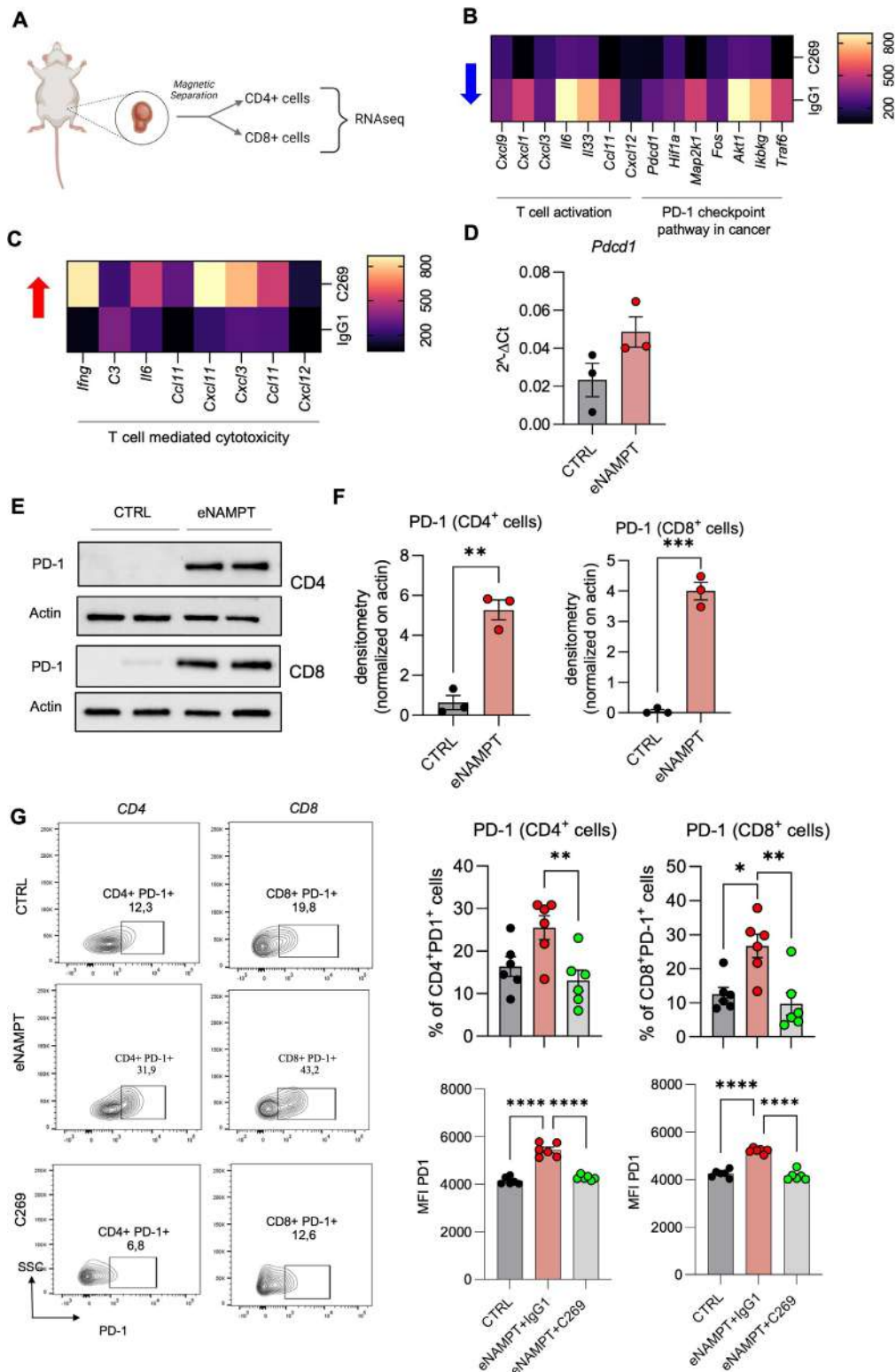


Figure 5 C269 shapes the immunophenotype of T-infiltrating cells. (A) Representative scheme of cells isolated from 4T1 tumor masses and subjected to RNAseq analysis. (B) Heat map and histogram depicting the downregulated genes by C269 treatment of CD4⁺ cells and relative GO analysis. (C) Heat map and histogram depicting the upregulated genes by C269 treatment of CD8⁺ cells and relative GO analysis. (D) *Pdcd1* (PD-1) expression by qPCR of T cells in response to eNAMPT (500 ng/mL). Mean ± SEM of three independent experiments. (E–F) Representative western blot and densitometry of PD-1 in total cell lysates of CD4⁺ and CD8⁺ T cells treated or untreated with rNAMPT for 24 hours and (G) quantification of PD-1 expression on T cells, pre-treated with eNAMPT for 24 hours and neutralized with C269 for other 24 hours. Mean ± SEM of three independent experiments. P value: **p < 0.01; ***p < 0.001. eNAMPT, extracellular nicotinamide phosphoribosyltransferase; GO, gene ontology; PD-1, programmed cell death protein 1; qPCR, quantitative PCR; RNAseq, RNA sequencing; rNAMPT, recombinant murine NAMPT; SSC, side scatter.

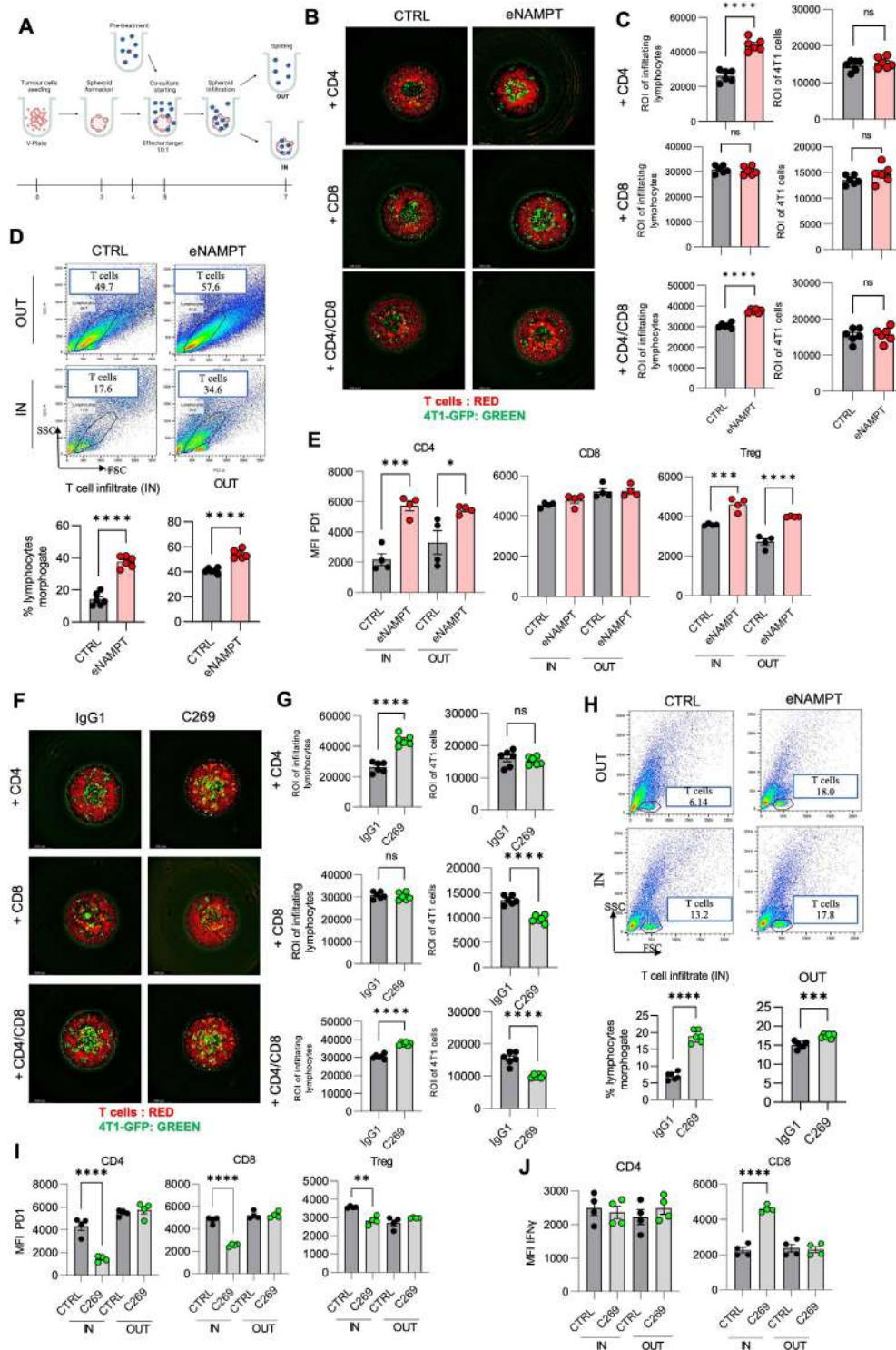


Figure 6 eNAMPT promotes immunosuppressive phenotype of tumor infiltrating lymphocytes within 4T1 spheroids. (A) Experimental scheme for experiments depicted in the figure. (B) Representative immunofluorescence images and (C) ROI quantification of 4T1-GFP cells (green) and lymphocytes (red) in the spheroid area. N=6, Mean±SEM of two independent experiments. (D) Flow cytometry analyses of spheroid T cell infiltration. N=6. Mean±SEM of two independent experiments. (E) MFI of PD-1 in the IN and OUT compartments. Mean±SEM of two independent experiments. (F) Representative immunofluorescence images and (G) ROI quantification of 4T1-GFP cells (green) and lymphocytes (red) in the spheroid area. Mean±SEM of three independent experiments. (H) Flow cytometry analyses of spheroid T-cell infiltration. N=6. Mean±SEM of three independent experiments. (I) MFI of PD-1 in the IN and OUT compartment of cocultured spheroids. Mean±SEM of three independent experiments. (J) MFI of IFN γ in the IN and OUT compartment of cocultured spheroids. Mean±SEM of three independent experiments. P value: * $p < 0.05$; ** $p < 0.01$; *** $p < 0.001$; **** $p < 0.0001$. eNAMPT, extracellular nicotinamide phosphoribosyltransferase; IFN, interferon; MFI, median fluorescence intensity; PD-1, programmed cell death protein 1, ROI, region on interest.

an increase in infiltrating CD8⁺ cells were found in the spheroid when treated with C269 compared with control.

This increase was now accompanied by a decrease in 4T1 cells, suggesting that antitumor cytotoxic activity was restored. In this case, though, infiltrating cells were significantly different when treated with C269, with significantly lower expression of PD-1 in infiltrating CD4⁺, CD8⁺ and Tregs compared with control, without showing any differences in CD73 and OX40 expression (online supplemental figure 9). For the former two populations, levels were also significantly lower to the lymphocytes which did not infiltrate in the same dish. As a further validation of activity, we also analyzed interferon gamma (IFN γ) expression, finding that infiltrating lymphocytes were IFN γ ⁺.

When comparing the effects of C269 *in vivo* and *in vitro* results are superimposable and therefore support the *in vitro* model used. On the contrary, while most data obtained with rNAMPT *in vitro* is in line with what expected from the effect of C269, it is surprising that rNAMPT increases the infiltrate (figure 6B–E), which is paradoxically the same effect given by the neutralization of the cytokine. *In vitro*, both C269 and rNAMPT increase CD4⁺ T cells, but there is a difference in their phenotype, as *in vitro* there is an increase in PD-1⁺ Tregs and this might be the reason for the increased infiltrate. Overall, therefore, the validity of the co-culture system used is limited to the contextualization of the effect of C269 and is hypothesis-generating for the effects of rNAMPT.

DISCUSSION

eNAMPT is the secreted form of the intracellular enzyme nicotinamide phosphoribosyltransferase, and is now a recognized cytokine released by tumors, by immune cells and by other cells (eg, adipocytes, fibroblasts, endothelial cells). A large number of reports have shown that this cytokine is elevated in the plasma of patients suffering from inflammatory disorders and cancer.^{15 35–37} Which cells are responsible for its release in cancer is unknown, although it is well known that tumor and immune cells show an increased expression of the intracellular form^{38 39} and that this can be released in a brefeldin-dependent and independent-manner.^{6 16 40} Recent evidence points to TLR4 as one of the receptors that eNAMPT engages once in the extracellular space, although this does not appear to be the sole receptor for eNAMPT. For example, we have recently shown that eNAMPT is able to skew M1 polarization of murine macrophages and trigger migration in either wild-type and TLR4 knock-out mice.¹⁶ *In vitro*, eNAMPT appears to have a pro-proliferative role^{41–44} and seems to promote epithelial-mesenchymal transition,^{45 46} but its contribution in pertinent *in vivo* cancer models is lacking.

In the present manuscript, we first confirmed that serum eNAMPT levels are also increased in allograft mouse models of triple negative breast cancer. Then, by using eNAMPT neutralizing antibodies (C269 and

ALT-200), we showed that restoring the levels of this cytokine leads to a decreased tumor growth and metastatic potential. eNAMPT does not appear to sustain the growth of the tumor cell directly or decrease the susceptibility to cell death as neither the cytokine nor the antibody had an effect in two-dimensional or three-dimensional 4T1 cell cultures. These data are partly in contrast with literature data, in which in cultured cells the treatment with recombinant eNAMPT seems to alter proliferation, which may be attributable to different cell lines used *in vitro*.^{41–43} On the contrary, our data firmly showed that eNAMPT controls the expression of PD-L1 on tumors and of PD-1 on T lymphocytes and therefore that its neutralization leads to a restoration of antitumoral immune responses. We have previously shown that the intracellular form of this protein controls the mobilization of immature myeloid-derived suppressor cells and enhances their suppressive role, while in the present contribution, we find no impact of eNAMPT neutralization on myeloid cells. It is well-known that NAMPT is increased intracellularly in cancer cells and in cancer-associated immune cells.^{5 47 48} Furthermore, an intracellular increase of NAMPT and the consequent NAD burst has been also associated with IFN γ -induced PD-L1 expression in tumoral cells.^{38 48} This leads to the intriguing picture in which the intracellular NAMPT controls the bioenergetic requirements of the cancer cell fuelling its requirements for proliferation and the myeloid antitumoral response, and its release controls the lymphoid immune evasion. A tripartite synergic boost to tumor progression linked by the fact that the intracellular form is the source of the extracellular form, creating a spatial and temporal control of immune evasion in tumors. Of note, the control of the expression of PD-L1 on tumors and of PD-1 on T lymphocytes appear to be cell autonomous as it can be reproduced in cultured tumorous cells and in isolated T lymphocytes from healthy animals. Indeed, transcriptomic analysis of *ex vivo* isolated CD4⁺ lymphocytes showed a damping of the genes associated with the PD-1 pathway. In total accord with this, the characterization of the tumor microenvironment confirmed the ability of C269 to increase T cytotoxic cell (IFN γ ⁺ and GrzB⁺) activation, reducing the PD-1⁺ fraction, removing the brake against cytotoxic functions.⁴⁹ Moreover, C269 reduced the immunoregulatory properties of Tregs, as seen in the immunosuppressive assay and in the reduction of the IL10⁺CD73⁺ T regulatory population.

The control by eNAMPT of the PD-1/PD-L1 axis is supported by the lack of addictiveness on tumor growth or metastases when animals are co-treated with C269 and anti-PD-1/PD-L1 antibodies, although these experiments also suggest that a more complex loop exists whereby these checkpoint receptors have a positive feedback on circulating eNAMPT and blocking the PD-1/PD-L1 pathway abolishes the effect of C269 on the primary tumor, as circulating eNAMPT is no longer elevated.

In conclusion, an anti-eNAMPT antibody is able to specifically skew T-lymphocytes to restore antitumoral

immune responses, and this appears beneficial and a promising therapeutic intervention in TNBC.

Author affiliations

- ¹Department of Drug Sciences, Università degli Studi di Pavia, Pavia, Italy
²Department of Pharmaceutical Science, University of Eastern Piedmont, Novara, Italy
³Department of Medical Oncology and Hematology Unit, IRCCS Humanitas Research Hospital, Rozzano, Italy
⁴Department of Medicine, University of Arizona Health Sciences, Tucson, Arizona, USA
⁵Dipartimento di Scienze della Salute, Interdisciplinary Research Center of Autoimmune Diseases-IRCAD, Università del Piemonte Orientale, Novara, Italy
⁶Molecular Immunology Unit, Department of Research, Fondazione IRCCS Istituto Nazionale dei Tumori di Milano, Milan, Italy
⁷Neuro-Oncology Unit, Department of Clinical Neuroscience, Fondazione IRCCS Istituto Neurologico Carlo Besta, Milan, Italy

Correction notice This article has been corrected since it was first published online. The affiliation of Massimo Costanza has been updated to: Neuro-Oncology Unit, Department of Clinical Neuroscience, Fondazione IRCCS Istituto Neurologico Carlo Besta, Milan, Italy.

Twitter Giorgia Colombo @judygilmore09 and Mario Paolo Colombo @MrioPaoloColo1

Contributors The study was designed by GC, CT, SS and AAG. GC and CT did the experiments. GC, CT, SS and AAG discussed and interpreted findings. CT and GC directed the work and GC, CT and AAG wrote the manuscript. MA, FF and NF did the viability and wound healing experiments. AG generated a stable 4T1-GFP cell line. RDS provided human samples. JGNG provided the humanized anti-eNAMPT antibody. NC helped with in vivo experiments. PP performed flowcytometry analysis. MC performed immunosuppression assay. FC and MPC critically revised the final manuscript. All of the authors have seen and approved the final version of the manuscript. AAG is responsible for the overall content as guarantor.

Funding The research was supported by an AIRC grant to AAG (AIRC IG2018 21842) and SS (AIRC IG2018 22208; Project Code: 25323), a PRIN grant from the Italian Ministry of Health to AAG (Ministero dell'Università e della Ricerca PRIN 2017 CBNCYT). An AIRC fellowship to GC (Project Code: 25323), a University of Pavia grant to CT (Università degli Studi di Pavia FRG-2019/2020), a Cariplo Foundation grant to CT (Fondazione Cariplo 2020-3598) and a PRIN grant from the Italian Ministry of Health to CT (Ministero dell'Università e della Ricerca PRIN 2020SEMP22).

Competing interests No, there are no competing interests.

Patient consent for publication Not applicable.

Provenance and peer review Not commissioned; externally peer reviewed.

Data availability statement Data are available upon reasonable request. The RNAseq data have been deposited in the Gene Expression Omnibus (GEO) database under the accession GSE223539.

Supplemental material This content has been supplied by the author(s). It has not been vetted by BMJ Publishing Group Limited (BMJ) and may not have been peer-reviewed. Any opinions or recommendations discussed are solely those of the author(s) and are not endorsed by BMJ. BMJ disclaims all liability and responsibility arising from any reliance placed on the content. Where the content includes any translated material, BMJ does not warrant the accuracy and reliability of the translations (including but not limited to local regulations, clinical guidelines, terminology, drug names and drug dosages), and is not responsible for any error and/or omissions arising from translation and adaptation or otherwise.

Open access This is an open access article distributed in accordance with the Creative Commons Attribution Non Commercial (CC BY-NC 4.0) license, which permits others to distribute, remix, adapt, build upon this work non-commercially, and license their derivative works on different terms, provided the original work is properly cited, appropriate credit is given, any changes made indicated, and the use is non-commercial. See <http://creativecommons.org/licenses/by-nc/4.0/>.

ORCID iD

Giorgia Colombo <http://orcid.org/0000-0002-8280-2589>

REFERENCES

- Jiang Y, Chen M, Nie H, *et al.* PD-1 and PD-L1 in cancer Immunotherapy: clinical implications and future considerations. *Hum Vaccin Immunother* 2019;15:1111–22.
- Kotanides H, Li Y, Malabunga M, *et al.* Bispecific targeting of PD-1 and PD-L1 enhances T-cell activation and antitumor immunity. *Cancer Immunol Res* 2020;8:1300–10.
- Cui X, Jia H, Xin H, *et al.* A novel Bispecific antibody targeting PD-L1 and VEGF with combined anti-tumor activities. *Front Immunol* 2021;12:778978.
- McGowan E, Lin Q, Ma G, *et al.* PD-1 disrupted CAR-T cells in the treatment of solid tumors: promises and challenges. *Biomedicine & Pharmacotherapy* 2020;121:109625.
- Travelli C, Consonni FM, Sangaletti S, *et al.* Nicotinamide Phosphoribosyltransferase acts as a metabolic gate for mobilization of myeloid-derived Suppressor cells. *Cancer Research* 2019;79:1938–51.
- Grolla AA, Torretta S, Gnemmi I, *et al.* Nicotinamide Phosphoribosyltransferase (NAMPT/PBEF/Visfatin) is a Tumoural cytokine released from Melanoma. *Pigment Cell Melanoma Res* 2015;28:718–29.
- Galli U, Colombo G, Travelli C, *et al.* Recent advances in NAMPT inhibitors: A novel Immunotherapeutic strategy. *Front Pharmacol* 2020;11:656.
- Garten A, Schuster S, Penke M, *et al.* Physiological and pathophysiological roles of NAMPT and NAD metabolism. *Nat Rev Endocrinol* 2015;11:535–46.
- Sun Z, Lei H, Zhang Z. Pre-B cell colony enhancing factor (PBEF), a cytokine with multiple physiological functions. *Cytokine Growth Factor Rev* 2013;24:433–42.
- Samal B, Sun Y, Stearns G, *et al.* Cloning and characterization of the cDNA Encoding a novel human pre-B-cell colony-enhancing factor. *Mol Cell Biol* 1994;14:1431–7.
- Revollo JR, Körner A, Mills KF, *et al.* Nampt/PBEF/Visfatin regulates insulin secretion in beta cells as a systemic NAD Biosynthetic enzyme. *Cell Metabolism* 2007;6:363–75.
- Dalamaga M, Christodoulatos GS, Mantzoros CS. The role of extracellular and intracellular Nicotinamide Phosphoribosyltransferase in cancer: diagnostic and therapeutic perspectives and challenges. *Metabolism* 2018;82:72–87.
- Sun BL, Sun X, Casanova N, *et al.* Role of secreted extracellular Nicotinamide Phosphoribosyltransferase (eNAMPT) in prostate cancer progression: novel biomarker and therapeutic target. *EBioMedicine* 2020;61:103059.
- Moschen AR, Kaser A, Enrich B, *et al.* Visfatin, an Adipocytokine with proinflammatory and Immunomodulating properties. *J Immunol* 2007;178:1748–58.
- Colombo G, Clemente N, Zito A, *et al.* Neutralization of extracellular NAMPT (Nicotinamide Phosphoribosyltransferase) ameliorates experimental murine colitis. *J Mol Med* 2020;98:595–612.
- Colombo G, Travelli C, Porta C, *et al.* Extracellular Nicotinamide Phosphoribosyltransferase BOOSTS IFN γ -induced macrophage polarization independently of Tlr4. *iScience* 2022;25:104147.
- Audrito V, Serra S, Brusa D, *et al.* Extracellular Nicotinamide Phosphoribosyltransferase (NAMPT) promotes M2 macrophage polarization in chronic lymphocytic leukemia. *Blood* 2015;125:111–23.
- Camp SM, Ceco E, Evenoski CL, *et al.* Unique toll-like receptor 4 activation by NAMPT/PBEF induces NF κ B signaling and inflammatory lung injury. *Sci Rep* 2015;5:13135.
- Van den Bergh R, Morin S, Sass HJ, *et al.* Monocytes contribute to differential immune pressure on R5 versus X4 HIV through the Adipocytokine Visfatin/NAMPT. *PLoS ONE* 2012;7:e35074.
- Torretta S, Colombo G, Travelli C, *et al.* The cytokine Nicotinamide Phosphoribosyltransferase (eNAMPT; PBEF; Visfatin) acts as a natural antagonist of C-C Chemokine receptor type 5 (Ccr5). *Cells* 2020;9:496.
- Managò A, Audrito V, Mazzola F, *et al.* Extracellular Nicotinamide Phosphoribosyltransferase binds toll like receptor 4 And mediates inflammation. *Nat Commun* 2019;10:4116.
- Ghanelalvar H, Shiri S, Kenarkoobi A, *et al.* Comparison of Visfatin levels in patients with breast cancer and endometrial cancer with healthy individuals: A systematic review and Meta-Analysis. *Health Sci Rep* 2022;5:e895.
- Assiri AMA, Kamel HFM. Evaluation of diagnostic and predictive value of serum Adipokines: Leptin, Resistin and Visfatin in postmenopausal breast cancer. *Obes Res Clin Pract* 2016;10:442–53.
- Zhu Y, Guo M, Zhang L, *et al.* Biomarker triplet NAMPT/VEGF/Her2 as a de novo detection panel for the diagnosis and prognosis of human breast cancer. *Oncol Rep* 2016;35:454–62.

- 25 Kilkeny C, Browne WJ, Cuthill IC, *et al.* Improving Bioscience research reporting: the ARRIVE guidelines for reporting animal research. *PLoS Biol* 2010;8:e1000412.
- 26 Bellenghi M, Talarico G, Botti L, *et al.* Scd5-dependent inhibition of SPARC secretion hampers metastatic spreading and favors host immunity in a TNBC murine model. *Oncogene* 2022;41:4055–65.
- 27 Revell AD, Wang D, Boyd MA, *et al.* The development of an expert system to predict virological response to HIV therapy as part of an online treatment support tool. *AIDS* 2011;25:1855–63.
- 28 Zambelli F, Pesole G, Pavesi G. Pscan: finding over-represented transcription factor binding site motifs in sequences from Co-regulated or Co-expressed genes. *Nucleic Acids Res* 2009;37:W247–52.
- 29 Courau T, Bonnereau J, Chicoteau J, *et al.* Cocultures of human colorectal tumor Spheroids with immune cells reveal the therapeutic potential of MICA/B and Nkg2A targeting for cancer treatment. *J Immunother Cancer* 2019;7:74.
- 30 Quijada H, Bermudez T, Kempf CL, *et al.* Endothelial eNAMPT Amplifies pre-clinical acute lung injury: efficacy of an eNAMPT-Neutralising Monoclonal antibody. *Eur Respir J* 2021;57:2002536.
- 31 Sun BL, Tang L, Sun X, *et al.* A Humanized Monoclonal antibody targeting extracellular Nicotinamide Phosphoribosyltransferase prevents aggressive prostate cancer progression. *Pharmaceuticals (Basel)* 2021;14:1322.
- 32 Grolla AA, Miggiano R, Di Marino D, *et al.* A Nicotinamide Phosphoribosyltransferase-GAPDH interaction sustains the stress-induced NMN/NAD⁺ salvage pathway in the nucleus. *J Biol Chem* 2020;295:3635–51.
- 33 Giancchetti E, Fierabracci A. Inhibitory receptors and pathways of lymphocytes: the role of PD-1 in Treg development and their involvement in Autoimmunity Onset and cancer progression. *Front Immunol* 2018;9:2374.
- 34 Rupp T, Genest L, Babin D, *et al.* CTLA-4 and anti-PD-1 Immunotherapies repress tumor progression in Preclinical breast and colon model with independent regulatory T cells response. *Transl Oncol* 2022;20:101405.
- 35 Armandi A, Colombo G, Rosso C, *et al.* The predictive role of extracellular NAPRT for the detection of advanced fibrosis in biopsy-proven non-alcoholic fatty liver disease. *Int J Mol Sci* 2023;24:1172.
- 36 Grolla AA, Travelli C, Genazzani AA, *et al.* Extracellular Nicotinamide Phosphoribosyltransferase, a new cancer Metabokine. *Br J Pharmacol* 2016;173:2182–94.
- 37 Colombo G, Caviglia GP, Ravera A, *et al.* NAMPT and NAPRT serum levels predict response to anti-TNF therapy in inflammatory bowel disease. *Front Med (Lausanne)* 2023;10:1116862.
- 38 Wang Y, Wang F, Wang L, *et al.* NAD⁺ supplement potentiates tumor-killing function by rescuing defective TUB-mediated NAMPT transcription in tumor-infiltrated T cells. *Cell Reports* 2021;36:109516.
- 39 Barba C, Ekiz HA, Tang WW, *et al.* Interferon gamma-inducible NAMPT in Melanoma cells serves as a mechanism of resistance to enhance tumor growth. *Cancers (Basel)* 2023;15:1411.
- 40 Yoshida M, Satoh A, Lin JB, *et al.* Extracellular Vesicle-contained eNAMPT delays aging and extends LifeSpan in mice. *Cell Metab* 2019;30:329–42.
- 41 Patel ST, Mistry T, Brown JEP, *et al.* A novel role for the Adipokine Visfatin/pre-B cell colony-enhancing factor 1 in prostate carcinogenesis. *Peptides* 2010;31:51–7.
- 42 Buldak RJ, Gowarzewski M, Buldak L, *et al.* Viability and oxidative response of human colorectal HCT-116 cancer cells treated with Visfatin/eNamp in vitro. *J Physiol Pharmacol* 2015;66:557–66.
- 43 Park H-J, Kim S-R, Kim SS, *et al.* Visfatin promotes cell and tumor growth by Upregulating Notch1 in breast cancer. *Oncotarget* 2014;5:5087–99.
- 44 Gholinejad Z, Kheiripour N, Nourbakhsh M, *et al.* Extracellular NAMPT/Visfatin induces proliferation through Erk1/2 and AKT and inhibits apoptosis in breast cancer cells. *Peptides* 2017;92:9–15.
- 45 Soncini D, Caffa I, Zoppoli G, *et al.* Nicotinamide Phosphoribosyltransferase promotes epithelial-to-Mesenchymal transition as a soluble factor independent of its enzymatic activity. *J Biol Chem* 2014;289:34189–204.
- 46 Cheng G, Liu C, Sun X, *et al.* Visfatin promotes Osteosarcoma cell migration and invasion via induction of epithelial-Mesenchymal transition. *Oncol Rep* 2015;34:987–94.
- 47 Pylaeva E, Harati MD, Spyra I, *et al.* NAMPT signaling is critical for the Proangiogenic activity of tumor-associated neutrophils. *Int J Cancer* 2019;144:136–49.
- 48 Lv H, Lv G, Chen C, *et al.* NAD⁺ metabolism maintains inducible PD-L1 expression to drive tumor immune evasion. *Cell Metab* 2021;33:110–27.
- 49 Ahn E, Araki K, Hashimoto M, *et al.* Role of PD-1 during Effector Cd8 T cell differentiation. *Proc Natl Acad Sci U S A* 2018;115:4749–54.

Correction: Extracellular nicotinamide phosphoribosyltransferase (eNAMPT) neutralization counteracts T cell immune evasion in breast cancer

Travelli C, Colombo G, Aliotta M, *et al.* Extracellular nicotinamide phosphoribosyltransferase (eNAMPT) neutralization counteracts T cell immune evasion in breast cancer. *J Immunother Cancer* 2023;11:e007010. doi: 10.1136/jitc-2023-007010

In this article, the affiliation of Massimo Costanza has been updated to: Neuro-Oncology Unit, Department of Clinical Neuroscience, Fondazione IRCCS Istituto Neurologico Carlo Besta, Milan, Italy.

Open access This is an open access article distributed in accordance with the Creative Commons Attribution Non Commercial (CC BY-NC 4.0) license, which permits others to distribute, remix, adapt, build upon this work non-commercially, and license their derivative works on different terms, provided the original work is properly cited, appropriate credit is given, any changes made indicated, and the use is non-commercial. See <http://creativecommons.org/licenses/by-nc/4.0/>.

© Author(s) (or their employer(s)) 2024. Re-use permitted under CC BY-NC. No commercial re-use. See rights and permissions. Published by BMJ.

J Immunother Cancer 2024;12:e007010corr1. doi:10.1136/jitc-2023-007010corr1

